ELSEVIER

Catalysis Today 50 (1999) 271–284

CATALYSIS TODAY

Textural and phase stability of $Ce_xZr_{1-x}O_2$ mixed oxides under high temperature oxidising conditions

G. Colón[a], F. Valdivieso[a], M. Pijolat[a,*], R.T. Baker[b], J.J. Calvino[b], S. Bernal[b]

[a]*Centre SPIN, Ecole Nationale Supérieure des Mines, 158, Cours Fauriel, 42023, St.Etienne Cedex-2, France*
[b]*Departamento de Ciencia de Materiales, Ingeniería Metalúrgica y Química Inorgánica, Facultad de Ciencias, Universidad de Cádiz, Apdo. 40, Puerto Real, 11510, Cádiz, Spain*

Abstract

The textural and structural changes in several Ce–Zr mixed oxides were studied. Changes in the crystal size and specific surface area upon calcination were followed at 1223 K over time. Different gas compositions (O_2, CO_2 and H_2O) were employed during calcination in order to better understand the sintering process in the $Ce_xZr_{1-x}O_2$ system. From S_{BET} and mean crystal size (D) curves, we have tried to obtain the kinetic parameters. In order to do that, all curves were fitted using a mathematical expression which allows the derivative and then the kinetic rates for S_{BET} decrease and D increase with calcination time to be obtained. It was also possible to correlate these rates with the Ce content of the mixed oxide, and to obtain information about the influence of composition on the sintering process at the surface and the crystalline structure of the mixed oxides. Complementary HREM/TEM data are also presented. With the help of this technique, it has been possible to elucidate the morphological and crystallographic changes in the crystallites upon calcination of the samples under oxidising atmospheres.

Keywords: Textural and phase stability; Sintering process; Crystallographic changes

1. Introduction

It is now well established that ceria plays a number of critically important roles in automotive three-way catalytic converters for the removal of post-combustion pollutants [1–3]. However, pure CeO_2 alone is known to be poorly thermostable [4–7]. The loss in surface area is usually related to the changes in the pore structure and to crystallite growth. It is, therefore, very important to improve its textural stability. Doping with cations such as Al^{3+}, Zr^{4+} or Si^4 [8–10] may significantly improve the stability of the surface area of ceria at high temperature. Recently, a new generation of mixed oxides containing CeO_2 and ZrO_2 has been developed. In addition to enhanced redox properties, these mixed oxides exhibit good thermal resistance [11,12].

In a previous paper [13], we presented a complete textural and structural characterisation of a series of $Ce_xZr_{1-x}O_2$ oxides with Ce/Zr compositions ranging from 80/20 to 15/85. It was envisaged that both textural and structural properties were closely related to the composition and also to the thermal treatment, being observed that phase segregation could occur.

The aim of this work is to investigate the evolution of the textural and structural properties of these oxides

*Corresponding author. Fax: +334-77-42-00-00; e-mail: mpijolat@emse.fr

0920-5861/99/$ – see front matter
PII: S0920-5861(98)00509-4

when calcined at 1223 K, under several different wet oxidising gas atmospheres.

2. Experimental

Four different high surface area Ce/Zr mixed oxide samples provided by Rhodia were tested in the present study: these will be referred to hereafter as CZ-80/20, CZ-68/32, CZ-50/50 and CZ-15/85, where the ratio XX/YY refers to the Ce/Zr molar ratio in the oxides. They have been prepared by hydrothermal synthesis from nitrate precursors, followed by drying for 1 h at 100°C and calcination between 600°C and 750°C.

The specific surface area (S_{BET}) of starting and thermally aged oxide powders was measured by the BET method using N_2 adsorption/desorption at 77 K (Micrometrics ASAP 2000). In the starting samples, it was found to be 100, 110, 100, 106 and 95 $m^2\,g^{-1}$, respectively, from CZ-100/00 to CZ-15/85.

X-ray diffraction spectra were recorded on a Siemens D501 diffractometer (Cu K_α) and the acquisition conditions were 0.006° in step size and 5 s per step. The proportion of the different phases was obtained by using the intensities of lines (1 1 1) for CeO_2 and $Ce_xZr_{1-x}O_2$ ($x \geq 0.68$), and (1 0 1) for $Ce_xZr_{1-x}O_2$ ($x \leq 0.5$). The mean crystal size (D) in samples was calculated by using the line broadening analysis [14], according to the Warren and Averbach equation (peaks were fitted by using a Voigt function),

$$D = \frac{\lambda \cdot 180}{\pi \cdot \cos\theta \cdot \sqrt{L^2 - L_{ref}^2}},$$

L and L_{ref} being the line width at medium height (FWHM) of the sample and a reference material, respectively. The reference powder required by this method was prepared by annealing a CZ-100/0 sample at 1473 K during 140 h, followed by slow cooling to room temperature.

Calcination of Ce–Zr mixed oxides was carried out using a Pyrox B80 furnace equipped with an alumina tube and a West 2050 regulator. A thermocouple placed inside the alumina tube allowed the measurement of the temperature in the vicinity of the samples. The flowing gas was a mixture of Ar, O_2 and CO_2 at atmospheric pressure whose composition was adjusted by means of Brooks Shorate 150 flowmeters. The feed gas mixture was passed through a water saturator whose temperature was regulated in order to provide the required water vapour content. The four gas compositions employed in the experiments are summarised in Table 1. Prior to calcination, the furnace chamber was preheated to 1223 K, then evacuated to 5×10^{-1} Torr and the appropriate mixture introduced. The time required to introduce the sample and establish the appropriate calcination conditions did not exceed 8 min. At this time (t=0), the various calcination periods were started for several hours up to 15 h. In these studies, the temperature of calcination was fixed at 1223 K. The specific surface areas of the preheated samples (up to time t=0) were measured in order to have the initial value in the conditions of isothermal calcinations. They are given in column 5 of Table 2.

Table 1
Summary of the experiments carried out

Experiment No.	P_{O_2} (Torr)	P_{CO_2} (Torr)	P_{H_2O} (Torr)
1	10	100	10
2	100	10	10
3	100	100	10
4	200	10	10

Oxide samples of two different compositions (CZ-50/50 and CZ-68/32) after 1 h and after 15 h calcination treatment were studied by high resolution electron microscopy/transmission electron microscopy (HREM/TEM) using a JEOL 2000-EX instrument. The microscope was equipped with a top entry specimen holder and ion pumping system, operated at an accelerating voltage of 200 kV and gave a nominal structural resolution of 0.21 nm. Samples were prepared by dipping a holey carbon copper grid into an ultrasonic dispersion of the oxide powder in hexane.

Selected area electron diffraction (SAEDs) patterns and high resolution micrographs over a range of magnifications up to ×600 K were recorded. All diffraction spectra and micrograph negatives were developed chemically and then digitised, processed and analysed using the SEMPER 6+ software package. By measuring the size (longest apparent width) of a large number (300–400) of crystals from micrographs taken at a range of magnifications, crystal size distributions were obtained. High resolution micrographs, in which the internal crystal structure was well

Table 2
Fitting parameters obtained for D and S_{BET} functions

No. Experiments	Sample	D_0 (experimental)	D_0	R	S_0 (experimental)	S_0	R
1	CZ-100/0	282.0	311.37	0.994	36.13	36.13	0.994
	CZ-80/20	149.3	149.14	0.997	25.04	25.04	0.998
	CZ-68/32	135.5	138.93	0.971	40.77	40.78	0.997
	CZ-50/50	122.8	–	–	38.00	38.00	0.998
	CZ-15/85	140.6	140.51	0.999	52.07	52.06	0.999
2	CZ-100/0	274.0	273.94	0.995	36.68	36.68	0.998
	CZ-80/20	147.7	147.53	0.998	29.83	29.84	0.998
	CZ-68/32	134.6	134.42	0.994	39.27	39.28	0.999
	CZ-50/50	122.2	–	–	41.04	41.04	0.999
	CZ-15/85	142.2	157.39	0.994	49.25	49.25	0.999
3	CZ-100/0	245.2	244.87	0.995	42.4	42.19	0.998
	CZ-80/20	127.1	127.09	0.999	36.5	36.49	0.998
	CZ-68/32	125.4	125.44	0.996	47.0	47.06	0.998
	CZ-50/50	110.1	–	–	53.4	53.30	0.999
	CZ-15/85	125.0	124.92	0.997	55.7	55.72	0.999
4	CZ-100/0	262.7	262.58	0.999	37.1	37.13	0.998
	CZ-80/20	141.6	141.58	0.999	34.4	34.44	0.997
	CZ-68/32	132.5	132.59	0.986	36.8	36.79	0.996
	CZ-50/50	112.4	–	–	47.5	47.52	0.998
	CZ-15/85	141.2	141.23	0.999	40.3	40.35	0.999

defined, were used to generate digital diffraction patterns (DDPs).

2.1. Methods

From representations of mean crystal size and S_{BET} versus calcination time, we have obtained the mathematical expressions best describing the experimental curves. The fitting functions employed were:

$$D = D_0(1 + At)^n \quad \text{with } n > 0, \tag{1}$$

$$S = S_0(1 + At)^n \quad \text{with } n < 0, \tag{2}$$

where D_0 and S_0 represent D and S_{BET} values at time equal to 0; A and n were fitting parameters for these functions.

It is interesting to represent the derivative values versus the sample composition for different values of mean crystal size [dD/dt=f(D)]. To do this, we modified the mathematical function by extrapolation in order to make all of them start at the minimum value of D at time zero (D'_0). Thus we are able to have the values of the derivatives for each value of D (Fig. 1). This modified function would have the following expression:

$$D' = D'_0(1 + A'\tau)^n \quad \text{with } n > 0. \tag{3}$$

The relationship between A and A' is given by the expression

$$A' = \frac{A}{(D'_0/D_0)^{1/n}}. \tag{4}$$

From this, we are able to obtain $\mathrm{d}D'(\tau)/\mathrm{d}\tau$ as a function of D, for all the mixed oxides. The mathematical expression that gives the derivative values is as follows:

$$\frac{\mathrm{d}D'(\tau)}{\mathrm{d}\tau} = n \cdot D'_0 \cdot A' \cdot \left(\frac{D'(\tau)}{D'_0}\right)^{(n-1)/n}. \tag{5}$$

A similar mathematical expression for $\mathrm{d}S'_{BET}/\mathrm{d}\tau$ is obtained by following the same steps as described above. This procedure allows us to avoid the problem of differences in D_0 or S_0 when representing the variations of the rates versus the Ce content for a given value of the mean crystallite diameter or surface area.

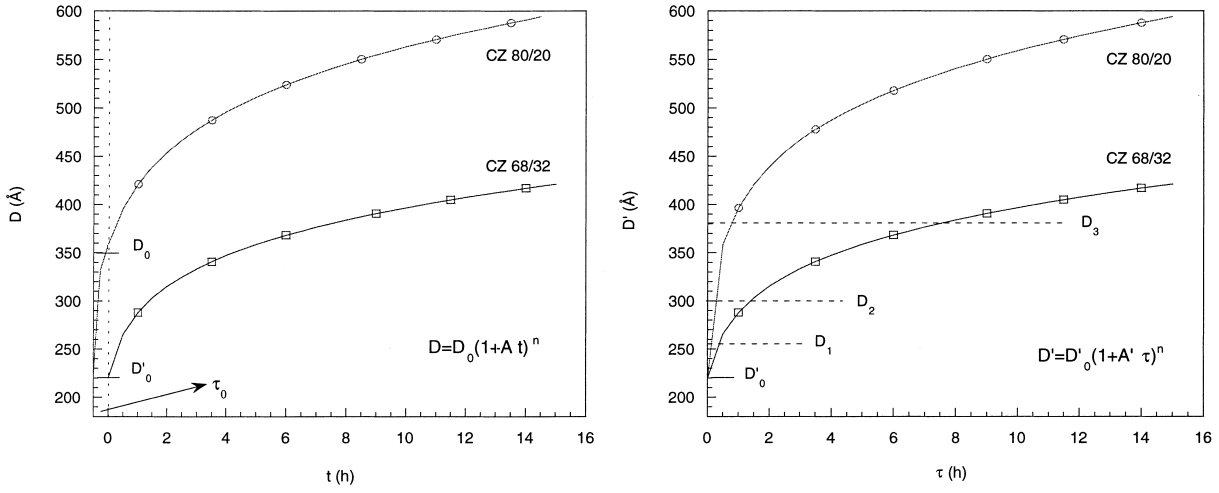

Fig. 1. Mathematical treatment of the experimental curves.

3. Results and discussion

3.1. BET and XRD studies

Complete textural and structural characterisation of the samples used here as starting materials are presented elsewhere [13]. It appears that the $Ce_xZr_{1-x}O_2$ system presents a solid solution structure in which the cation sub-lattice has cubic structure for $x \geq 0.68$ and tetragonal structure for $x \leq 0.5$. The presence of X-ray diffraction peaks of monoclinic ZrO_2 besides those of the tetragonal CZ-15/85 sample were also observed. Fig. 2(a)–(c) presents plots of D versus calcination time for several experiments carried out. We will show only these three as examples. Table 2 reports the values obtained for D_0 from XRD (column 3) and from fitting using Eq. (1) (column 4), as well as the correlation factor.

It is clear that CZ-100/0 undergoes a rapid crystallite growth process since D values increase significantly more than in the mixed oxide samples. Therefore, the crystallite growth process is retarded or disfavoured by the incorporation of Zr ions into the CeO_2 matrix. The samples can be classified according to their behaviour. We find that CZ-80/20 and CZ-15/85 samples present similar behaviours during calcination. On the other hand, CZ-68/32 and CZ-50/50 develop in a different way, mean crystal size values for CZ-68/32 increase only slightly with calcination time while for CZ-50/50, they remain almost constant in all cases. Apparently, there is no clear effect of gas composition on crystal growth in these samples.

By examination of the XRD peaks, we have found that CZ-50/50 presents phase segregation in all the experiments, even after only 1 h of calcination (Fig. 3). The new phases that appear gradually upon calcination correspond to phases whose compositions are approximately $Ce_{0.8}Zr_{0.2}O_2$ and $Ce_{0.2}Zr_{0.8}O_2$. This could explain the fact that D remained virtually constant in CZ-50/50, whereas the surface area decreased (cf. this point will be further discussed). Fig. 4(a)–(c) presents the evolution of the various phases present in CZ-50/50 with calcination time for different experiments. The percentage of each phase has been calculated from the intensities of main XRD peaks. It is clear that $Ce_{0.5}Zr_{0.5}O_2$ disappears progressively upon calcination, while the percentages of the new phases increase. A slight influence of oxygen partial pressure on the rate of appearance of the new phases can also be noted. It seems that a high CO_2 content stabilizes the original solid solution, $Ce_{0.50}Zr_{0.5}O_2$. In order to clarify the particular effect of O_2 and CO_2, we performed several calcinations by flowing separately O_2/Ar and CO_2/Ar at different partial pressures (100 and 200 Torr). We have observed that after 15 h of calcination (Fig. 5), results indicate a clear dependence of the amount of segregated new phases on the O_2 partial pressure. The higher the oxygen partial pressure, the

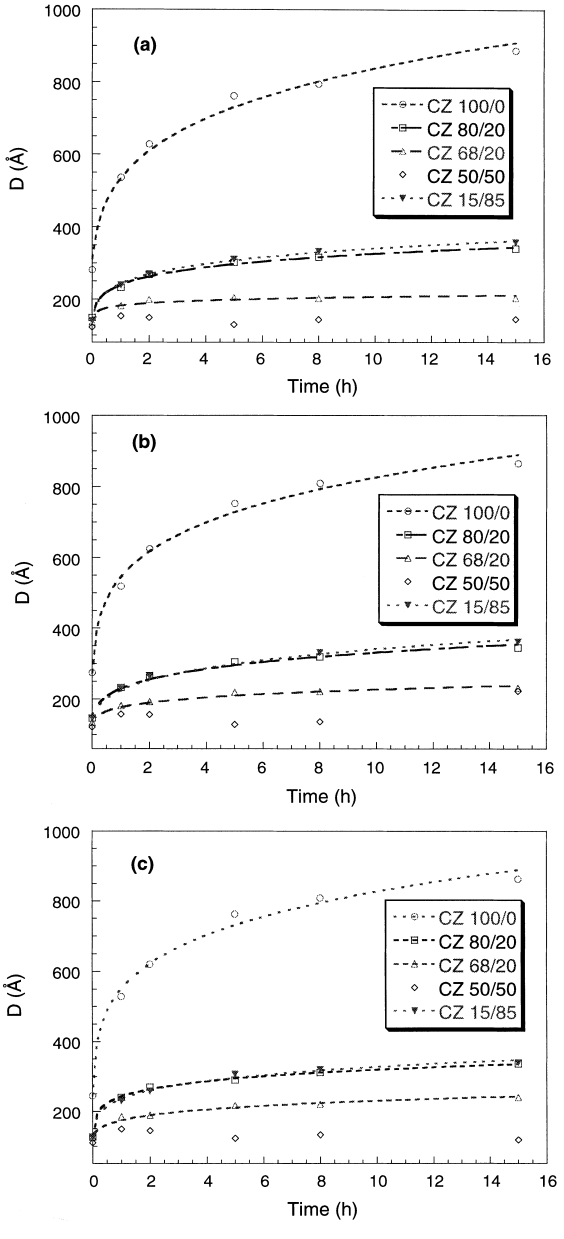

Fig. 2. Mean crystal size values during calcination at 1223 K for $Ce_xZr_{1-x}O_2$ system: (a) $P(O_2)$=10 Torr and $P(CO_2)$=100 Torr; (b) $P(O_2)$=100 Torr and $P(CO_2)$=10 Torr; and (c) $P(O_2)$=100 Torr and $P(CO_2)$=100 Torr, $P(H_2O)$=10 Torr in all cases.

higher the degree of segregation from the $Ce_{0.5}Zr_{0.5}O_2$ solid solution.

Phase segregation is also expected in the CZ-68/32 sample as we were able to establish in a previous work

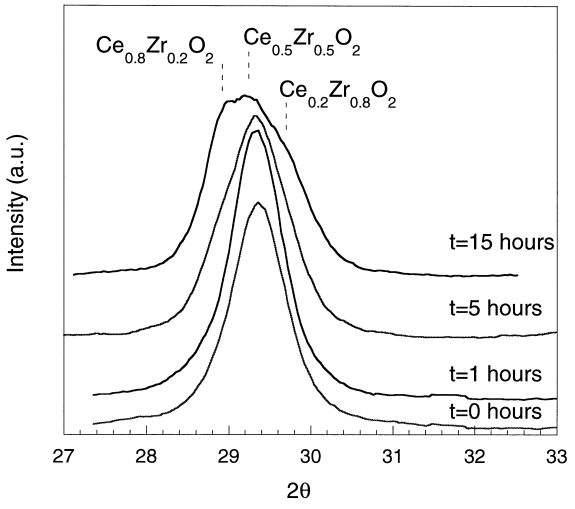

Fig. 3. Evolution of the (1 0 1) diffraction peak for CZ-50/50 calcined at 1223 K during the time for one of the experiments carried out.

from XRD data obtained by calcinating the as received powders at 1473 K [13], however, at the lower temperature of these experiments, it was not clearly evident. From these results, a different calcination behaviour of these two samples can be inferred. From the curves of *D* versus calcination time (Fig. 2(a)–(c)), it can be seen that, for the CZ-50/50 sample, the mean crystal size reached a maximum value in the first stages of the calcination process. After that crystal growth did not proceed any more, whereas phase demixtion does occur. It seems that, once $Ce_{0.5}Zr_{0.5}O_2$ has reached a critical mean crystal size of around 150 Å, the favoured process is the segregation to phases more thermodynamically stable, that is $Ce_{0.8}Zr_{0.2}O_2$ and $Ce_{0.2}Zr_{0.8}O_2$ [13]. In the case of CZ-68/32, as this effect is not so clear at the temperature used here, it could be supposed that the critical crystal size for this process to occur is higher; however, it is clear that for this sample also the mean crystal size reaches an almost constant value during the last 7 h of calcination (see Fig. 2(a)–(c)), while a different type of profile was obtained for the CZ-80/20 and CZ-15/85 samples in which the crystallites grow continuously with passing calcination time. The HREM results presented in Section 3.2 will give further evidence of the presence of more than one phase in the CZ-68/32 sample after 15 h of calcination

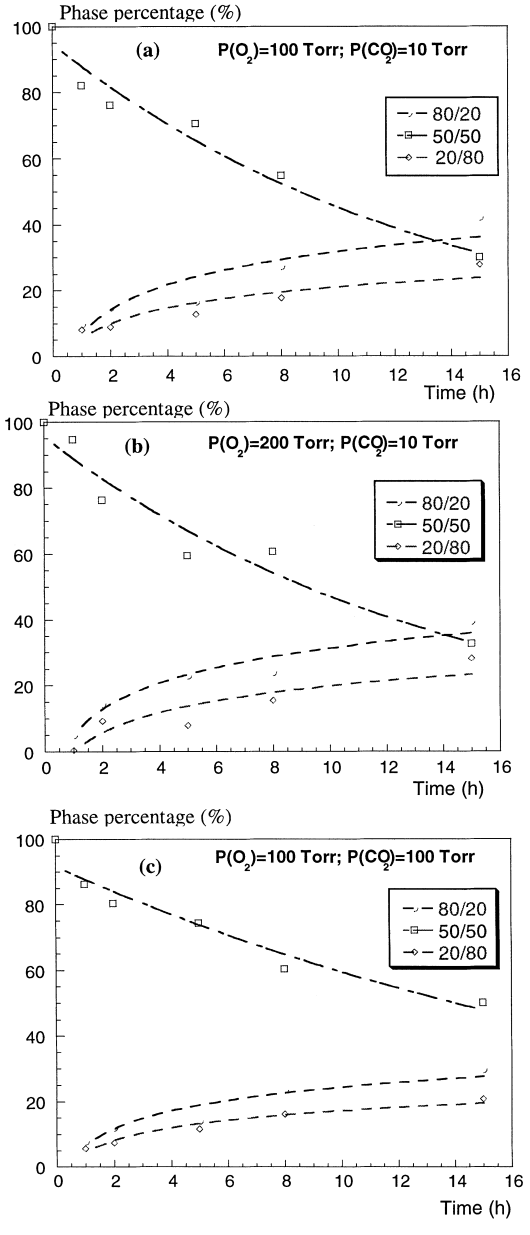

Fig. 4. Phase percentages in CZ-50/50 for different experiments, $P(H_2O)$=10 Torr in all cases.

at 1223 K, as in the CZ-50/50 sample after only 1 h of calcination.

Fig. 6(a)–(c) shows the variations of surface area with calcination time. The initial values, S_0, of all the samples are rather low compared to those of the starting powders (see also Table 2); this is due to a very fast surface area loss during the short period necessary to establish the isothermal and isobaric conditions of calcination. For each Ce/Zr composition, these values vary according to the gaseous conditions (cf. Tables 1 and 2) which show that the atmosphere of calcination influences the initial loss in surface area, whereas there is no evidence for significant effects on the evolution of the specific surface area versus time at 1223 K (similar curves were obtained with 2 Torr of water vapour instead of 10). It can be observed in Fig. 6 that the surface area suffers a drastic decrease during the first hour of calcination, arriving at a rather stable value after the second hour. We can also see that, of the mixed oxides, the CZ-80/20 presents the lowest surface area. By fitting the plots using Eq. (2), we obtained the parameters for the surface area rate (Table 2).

Although an increase of crystal size would usually be expected to accompany a decrease in surface area, such an increase is apparently not observed for the CZ-50/50 sample. We have to take into account that the D values have been calculated from XRD data for the $Ce_{0.5}Zr_{0.5}O_2$ phase only and that the surface area corresponds to the whole mixture of (Ce, Zr)O_2 phases present in the CZ-50/50 sample. It seems that the surface area decrease is related to the increasing percentage of the new phases while D [···] of the $Ce_{0.5}Zr_{0.5}O_2$ phase alone remains roughly constant. It seems likely that the demixtion process leads to the formation of grain boundaries between newly-formed domains of the new phases and the original $Ce_{0.5}Zr_{0.5}O_2$ particle. In this way the surface area of the whole sample measured by BET would decrease during calcination, while the D values detected in XRD, and which relate only to the $Ce_{0.5}Zr_{0.5}O_2$ phase, would remain roughly constant or, indeed, decrease.

In order to understand better the mechanism of sintering, we have tried to correlate dD/dt with the Ce content in the samples for several mean crystal size values. As explained before, by modification of the $D(t)$ function, we have calculated the values of $dD'/d\tau$ for each sample Eq. (5). In Fig. 7(a)–(c), calculated $dD'/d\tau$ values are plotted against the Ce content for several mean crystal size values. The values for CZ-100/0 were not included since we have focussed our attention on the effect of the incorporation of Zr into the CeO_2 lattice. It should only be mentioned that

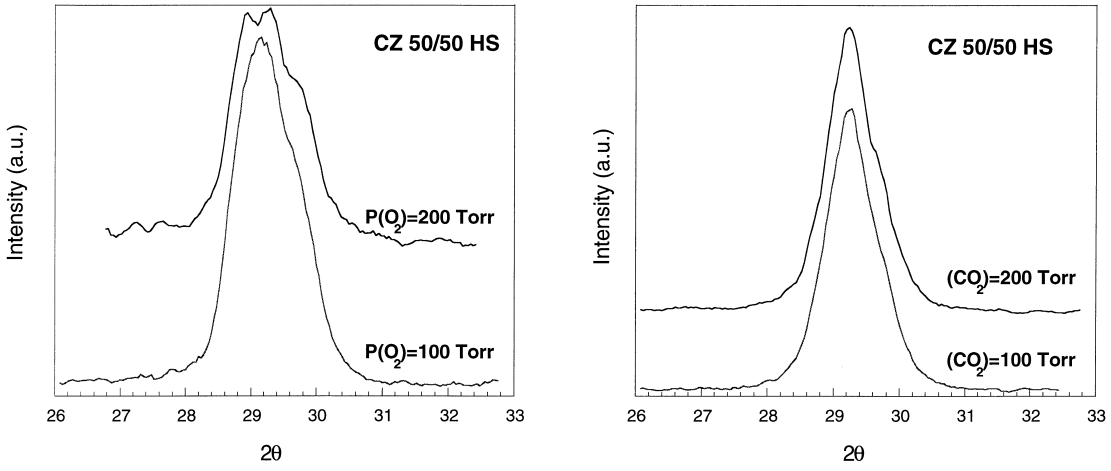

Fig. 5. Effect of O_2 and CO_2 on the evolution of (1 0 1) diffraction peak for CZ-50/50 sample calcined at 1223 K during 15 h.

CZ-100/0 presents the highest values of $dD'/d\tau$, as was inferred previously from Fig. 1. We have considered also that $dD'/d\tau$ for the CZ-50/50 mixed oxide is approximately zero since its D values are almost constant. From the plots, it can be observed that $dD'/d\tau$ always presents maximum values in the cases of CZ-80/20 and CZ-15/85 samples. This implies that, for these samples, crystal growth progresses more rapidly than that of the others. It is clear from kinetic considerations that these samples would be the less interesting compositions in the $Ce_xZr_{1-x}O_2$ system, in the sense that they suffer a rapid coalescence. This does not happen in CZ-50/50 (and to a lesser extent in CZ-68/32), which we explain by the demixtion process occurring as soon as a critical crystal size is reached. The fact that crystal growth nearly stops and phase transformation occurs from a critical crystal size has also been observed in the case of ZrO_2 [15], when fine particles of tetragonal zirconia are transformed into the monoclinic form.

In fact, after calcining Ce–Zr mixed oxides at 1473 K for 140 h in a previous study [13], CZ-68/32 and CZ-50/50 samples both gave XRD patterns with diffraction peaks which could be assigned to two solid solutions with approximately 80% and 12% in CeO_2, without any trace of the original solid solutions. However, CZ-80/20 and CZ-15/85 did not undergo such changes in their phase composition after the same severe calcination treatment, the only change being that in CZ-15/85, an almost negligible amount of ZrO_2 was detected which tended to disappear upon calcination.

Similar calculations have also been made for the surface area. We have arrived at similar curves, but in this case representing $-dS'/d\tau$ versus solid solution composition for each value of surface area (Fig. 8(a)–(c)). It can be observed that a maximum of $-dS'/d\tau$ for the solid solution CZ-80/20 is always found, for each surface area value and independently of the gas mixture. Thus, it is in this mixed oxide composition that the sintering process is fastest, and therefore, that the textural stability is lowest. However, from the point of view of thermodynamic stability, the CZ-50/50 and CZ-68/32 compositions show that a demixtion process occurs which could in turn modify the redox properties of the oxide.

3.2. *Electron microscopy*

HREM/TEM studies were performed on CZ-68/32 and CZ-50/50 samples after 1 and 15 h calcination time. Fig. 9 shows the crystal size distributions for these samples. A correction has been applied to the frequency of the histograms for crystal volume in order that the same volume (or mass, assuming constant density) of crystals gives rise to a bar of constant height independent of the crystal size fraction it represents. In this form, the data can be compared with those obtained by analysis of XRD spectra. A consequence of this method is the appearance of either

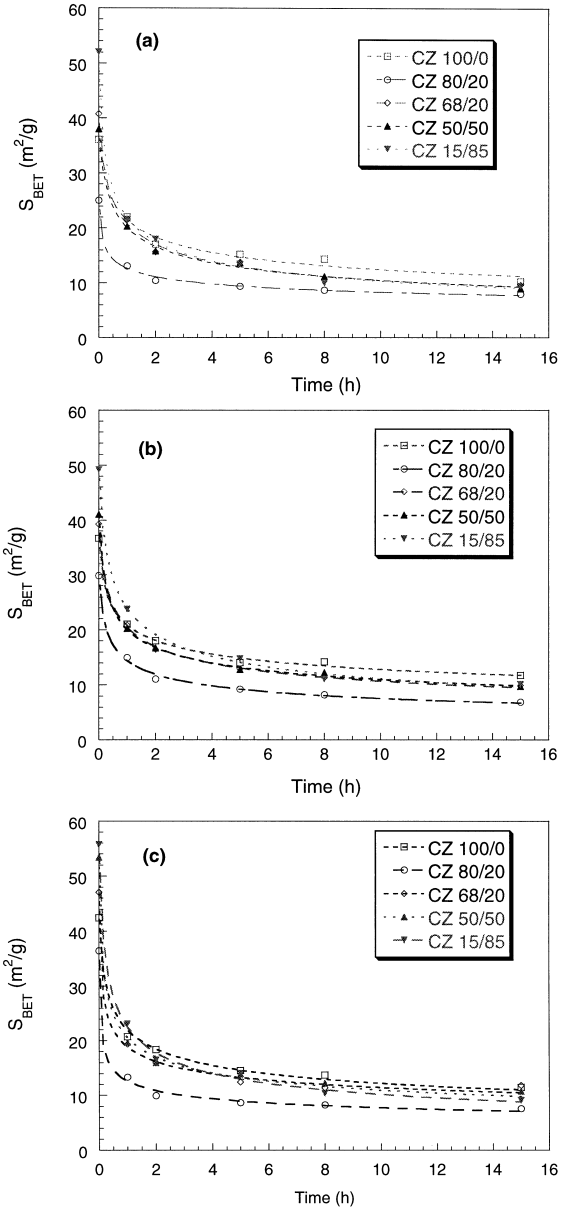

Fig. 6. BET surface area values during calcination at 1223 K for $Ce_xZr_{1-x}O_2$ system: (a) $P(O_2)$=10 Torr and $P(CO_2)$=100 Torr; (b) $P(O_2)$=100 Torr and $P(CO_2)$=10 Torr; and (c) $P(O_2)$=100 Torr and $P(CO_2)$=100 Torr, $P(H_2O)$=10 Torr in all cases.

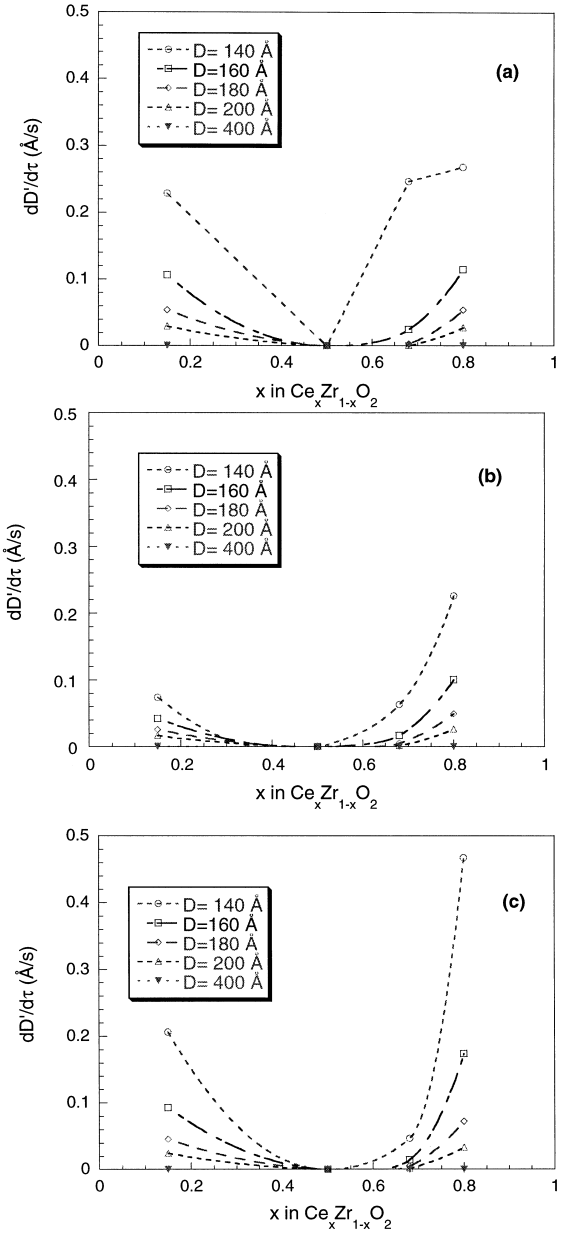

Fig. 7. Evolution of $dD'/d\tau$ against CeO_2 composition in $Ce_xZr_{1-x}O_2$ for different D values: (a) $P(O_2)$=10 Torr and $P(CO_2)$=100 Torr; (b) $P(O_2)$=100 Torr and $P(CO_2)$=10 Torr; and (c) $P(O_2)$=100 Torr and $P(CO_2)$=100 Torr, $P(H_2O)$=10 Torr in all cases.

no or very large bars at the largest crystal sizes where the number of crystals measured is very small, but their volumes, and so their impact on the histogram are very large.

For both sample compositions, mean crystal size increases only slightly and the crystal size distribution broadens, on increasing calcination time. Mean crystal

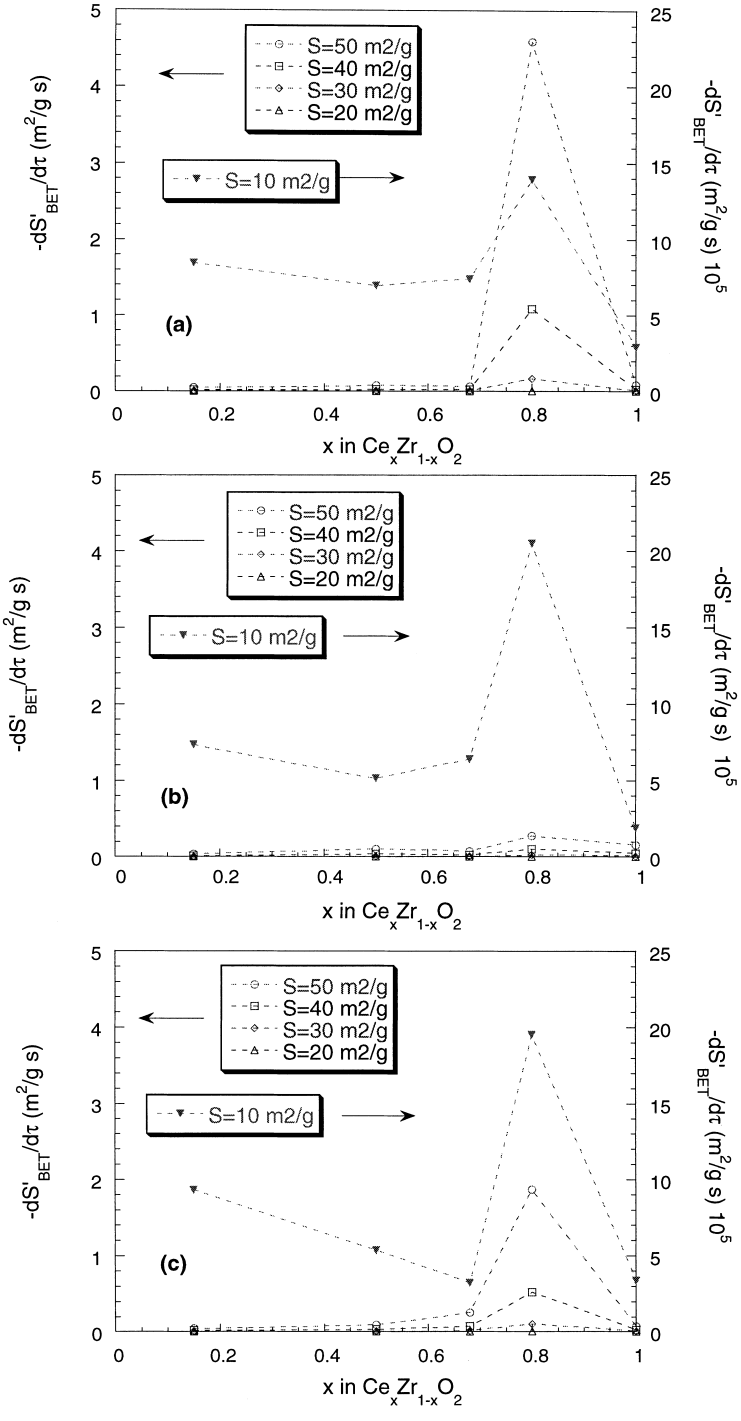

Fig. 8. Evolution of $-dS'/d\tau$ against CeO_2 composition in $Ce_xZr_{1-x}O_2$ for different S_{BET} values: (a) $P(O_2)$=10 Torr and $P(CO_2)$=100 Torr; (b) $P(O_2)$=100 Torr and $P(CO_2)$=10 Torr; and (c) $P(O_2)$=100 Torr and $P(CO_2)$=100 Torr, $P(H_2O)$=10 Torr in all cases.

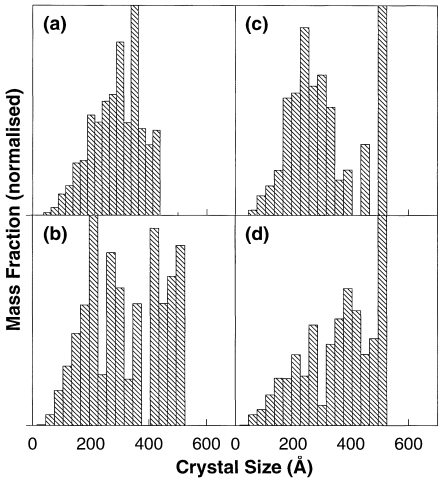

Fig. 9. Crystal size distributions obtained from HREM micrographs for CZ-50/50 after (a) 1 and (b) 15 h calcination; and for CZ-68/32 after (c) 1 and (d) 15 h calcination.

size increases slightly more for CZ-68/32 (290–342 Å) than for CZ-50/50 (276–307 Å). An increase in the amount of small and of large crystals at the expense of those of intermediate size appears to take place. This is much more marked for the CZ-50/50 sample, for which a bimodal crystal size distribution might be inferred after the 15 h treatment. These values of mean crystal size are higher than those obtained from XRD. It is possible that part of this difference can be explained by systematic differences between the two methods. However, the difference between the values is wider for the CZ-50/50 samples. This may indicate the presence of microdomains in some crystals of this composition in particular and possibly also in the CZ-68/32, although to a lesser extent. These microdomains would not necessarily have been detected in TEM, but would have had an influence on the XRD peak widths.

Intermediate magnification images of the CZ-50/50 and CZ-68/32 samples, after 1 h and after 15 h calcination treatment, are presented in Fig. 10. In both samples, the crystals generally formed into aggregates in which crystals not completely overlapped by others were quite rare. Crystal shape and size did not change markedly between samples treated for 1 and 15 h for either sample composition. However, an interesting change was noticed. After 15 h calcination, a significant number of crystals displayed a system of approximately parallel high contrast light and dark bands extending across their surfaces. An example can be seen in the bottom right-hand corner of Fig. 10(b) and more clearly in a high magnification micrograph of a different crystal in Fig. 11. The ‘wavelength’ of these features, at about 4 nm, was large compared to the dimensions of the crystallographic unit cell. This phenomenon was much more common for CZ-50/

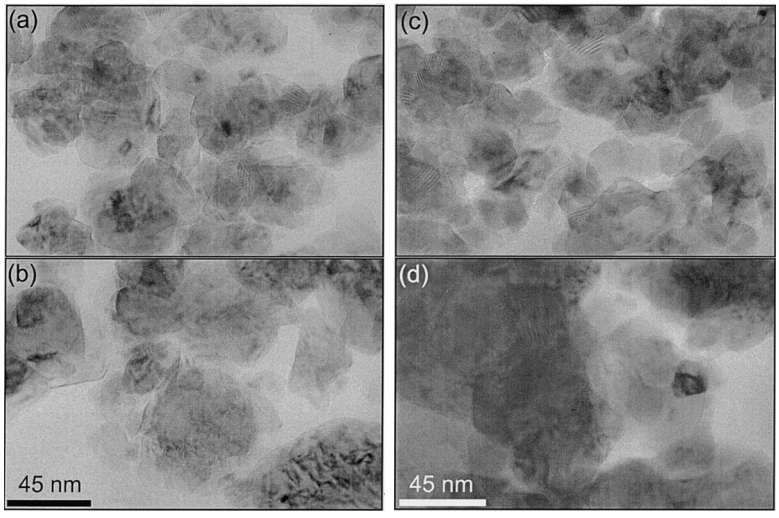

Fig. 10. Intermediate magnification images of CZ-50/50 after (a) 1 and (b) 15 h calcination; and for CZ-68/32 after (c) 1 and (d) 15 h calcination.

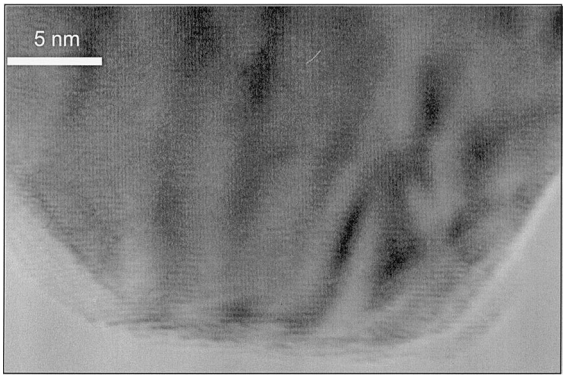

Fig. 11. HREM micrograph of crystal of CZ-50/50 after 15 h calcination showing broad surface bands.

50 than for CZ-68/32 and may be a diffraction phenomenon caused by the presence of a surface layer of different phase or crystallographic orientation to that of the supporting crystal. In fact, a narrow structure runs along almost the whole visible edge of the crystal in Fig. 11. This is of much lighter contrast than the main body of the crystal, but seems to be a continuation of it since horizontal lines seen clearly across the whole of the crystal seem also to continue into this peripheral structure.

Both experimental SAED patterns and DDPs derived from micrograph images showing crystals with well-defined bidimensional internal structure were analysed quantitatively and the resulting data compared with data held in crystallographic databases of the cubic (Fluorite), tetragonal and monoclinic phases of pure ZrO_2. Data for pure ZrO_2 were employed, since not all of the crystallographic parameters required to construct databases for the equivalent phases of Ce/Zr mixed oxides were available.

Representative experimental SAED patterns for each of the four samples are collected together in Fig. 12. These patterns are broadly consistent with a Fluorite (F) structure. However, it should be remembered that the tetragonal phases of Ce/Zr mixed oxides give rise to diffraction patterns which include spots at positions very similar to those of the F-phase. Further, the tetragonal patterns often differ from the F-pattern, only in that they include additional spots which are kinetic extinctions and so whose intensity may be very low or zero. Therefore, the tetragonal patterns may not be easily distinguished from the F-phase using SAED data alone (see previous work, [13]).

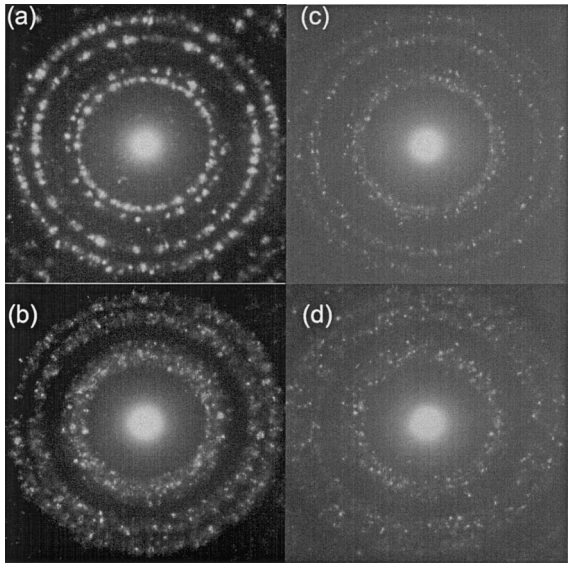

Fig. 12. Selected area electron diffractograms for CZ-50/50 after (a) 1 and (b) 15 h calcination; and for CZ-68/32 after (c) 1 and (d) 15 h calcination.

It is clear from the diffractograms presented in Fig. 12, however, that the number and/or concentration of new phases present increases with calcination time. After 1 h calcination treatment, the samples give patterns of concentric rings or narrow bands. However, after 15 h, these broaden into wide bands. This was confirmed quantitatively on analysis of the radial intensity of the patterns. Since no new rings were observed, this suggests the presence of a number of similar phases.

The monoclinic phase gives rise to a reasonably intense diffraction rings at spacings of about 5.1 and 3.7 Å. Several SAED patterns showed one or two spots at these spacings and a single agglomerate of crystals was found (in the CZ-50/50 sample after 15 h calcination) whose SAED pattern showed a very significant concentration of the monoclinic phase. However, these observations were isolated and were not considered statistically strong evidence for the existence of a significant concentration of monoclinic crystals.

For each of the four samples studied by HREM, several micrographs were selected in which the bidimensional crystal structure was well-defined. DPPs were generated from these images using a Fourier-transform technique. The resulting electron diffraction

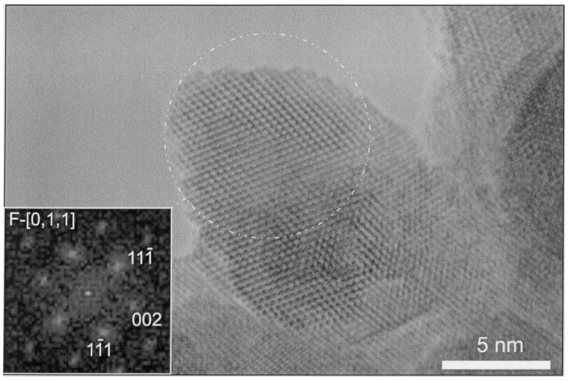

Fig. 13. HREM micrograph of crystal of CZ-68/32 after 1 h calcination with DDP (inset) indexed to the F-structure viewed along the [0,1,1] zone axis.

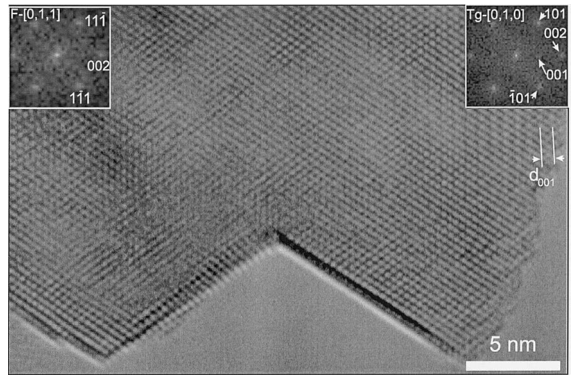

Fig. 14. HREM micrograph of crystal of CZ-50/50 after 1 h calcination. The left-half of the crystal gives a DDP (inset, top left) which can be indexed to the F-structure viewed along the [0,1,1] zone axis. The DDP from the right half (inset, top right) is best indexed to the tetragonal (*T*g) structure viewed along the [0,1,0] zone axis.

patterns were analysed quantitatively and compared with patterns of the Fluorite, tetragonal and monoclinic phases of ZrO_2.

For both CZ-50/50 and CZ-68/32 calcined for 1 h only, the majority of the DDPs could be indexed closely to the F-structure. These were generally seen in the [0,1,1] zone axis. This implies that the crystals have either the fluorite structure or a tetragonal structure indistinguishable from it because of the absence of the kinetic extinctions described above. Such a crystal (from the CZ-68/32 sample after 1 h treatment) is shown in Fig. 13 with the corresponding DDP inset. A variation on this theme is seen in the unusually shaped double crystal in Fig. 14 (CZ-50/50 after 1 h treatment). The left-half of the crystal gives rise to a DDP (inset, left corner) such as that described above which can be indexed to the F-[0,1,1] zone axis. The DDP pattern obtained from the right-half is aligned with the first pattern and is very similar. However, two clear new spots appear in addition. These are best indexed to ⟨0,0,1⟩ active kinetic extinctions in a tetragonal phase viewed in the [0,1,0] zone axis. The intensities of kinetic extinctions are sensitive to the optics of the microscope, the orientation, and thickness of the crystal and the nature of the exposed surface planes. This may explain why these two spots are not seen in the other half of the crystal.

Fig. 15 presents a further example of this (CZ-68/32 after 15 h calcination). Across most of the crystal, the simple fluorite pattern is generated in the DDP (inset top left). However, the region marked, at the

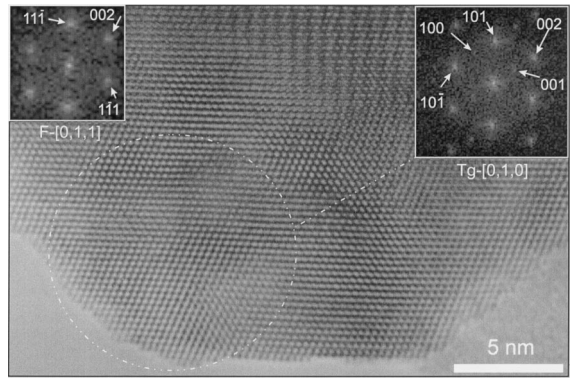

Fig. 15. HREM micrograph of crystal of CZ-68/32 after 15 h calcination. Most regions of the crystal give a DDP (inset, top left) which can be indexed to the F-structure viewed along the [0,1,1] zone axis. The DDP (inset, top right) from the circled region at the crystal edge, however, is best indexed to the tetragonal (*T*g) structure viewed along the [0,1,0] zone axis.

edge of the crystal, generates what appears to be a tetragonal pattern viewed along the [0,1,0] zone axis. The ⟨0,0,1⟩ and ⟨1,0,0⟩ kinetic extinctions are visible, even though the latter should have an intensity very close to zero according to dynamical calculations. It may be present due to the effects listed in the previous paragraph or to second order imaging effects, as described in a previous contribution [13], in which the ⟨100⟩ spots gain intensity during the imaging process at the objective lens. In effect, second-order

interactions between the spots ⟨001⟩ and ⟨10−1⟩, result in the transfer of intensity to the ⟨100⟩ in the imaging plane.

Therefore, there is a clear evidence for the presence of a tetragonal crystal phase in these two samples. This evidence is in the form of kinetic extinctions which may not always be active, and whose intensities may be sensitive to optical conditions and the geometry and alignment of the crystal viewed. This would explain the appearance of these spots only in part of the crystals imaged in Figs. 14 and 15. Taking into account the demixtion seen in XRD and the evidence for a surface layer in HREM, another feasible explanation is that the crystal phases are actually different. That is, that the unusually orientated joined crystals in Fig. 14 have different phases of different composition resulting from a demixtion as deduced from the XRD results. This would also explain their energetically unstable geometry. In Fig. 15, the crystal would be in an earlier stage of demixtion, the tetragonal phase seen only near the crystal edge.

4. Conclusions

It has been shown that Zr^{4+} incorporation into cubic CeO_2, retards the crystal growth process responsible for sintering. The rate of crystallite coalescence is maximum for CZ-100/0 (pure ceria) which presents much larger mean crystal size values than the mixed oxides. In the mixed oxides, for samples with intermediate Ce content (CZ-68/32 and CZ-50/50), crystal size increases only very slightly for CZ-68/32 and remains quite constant for CZ-50/50. At the same time, segregation of new phases has been detected for the CZ-50/50 sample (with strong indications for CZ-68/32).

A relationship between these two effects has been proposed. Crystal growth would take place until a certain critical mean crystal size is reached, when phase segregation would begin, forming thermodynamically more stable phases. This is in agreement with the bimodal crystal size distribution observed in TEM. In the case of CZ-50/50, the situation would progress from the tetragonal $Ce_{0.5}Zr_{0.5}O_2$ mixed oxide towards a mixture of the initial phase together with certain fractions of cubic $Ce_{0.8}Zr_{0.2}O_2$ and tetragonal $Ce_{0.2}Zr_{0.8}O_2$ mixed oxides. In the case of CZ-68/32 sample, this process seems to occur very slowly, probably due to a higher critical crystal size at the temperature of the experiment.

Then, from the point of view of crystal size and surface area, the higher thermal stability would correspond to these intermediate mixed oxides (CZ-68/32 and CZ-50/50), for which crystal size does not suffer a strong increase, but in which there is the possibility of demixtion into new phases. In all cases, however, mixed oxides were found to present better resistance against sintering than CeO_2.

The highest rate constant for the decrease of surface area corresponds to the CZ-80/20 sample. This, therefore, is the sample that possesses the lowest thermal stability in terms of surface area. Rates of decrease of the surface area for the rest of the samples were significantly lower than for CZ-80/20 and generally similar to each other.

By means of HREM/TEM analysis of samples CZ-58/32 and 50/50 calcinated at 1223 K, it has been found that the mean crystal size and breadth of the crystal size distribution change only slightly with calcination time after the initial 1 h. There appears to be a tendency towards a bimodal crystal size distribution with increasing calcination time. This might be explained by the demixtion of a new phase, forming small crystals, and formation of a surface layer and/or slow crystal growth, forming larger crystals.

The general, morphology of the crystals changes little between 1 h and 15 h of calcination treatment. However, an unusual system of broad interference bands occurs frequently on crystals of CZ-50/50 after 15 h calcination. This may be linked with the presence of a thin surface layer, perhaps of a demixing phase.

Experimental electron diffraction data suggest that the initial majority phase is a fluorite phase or a tetragonal phase indistinguishable using this method. SAED patterns imply an increase in the number and/or concentration of new phases similar to the initial majority phase with increasing calcination time. There is a clear evidence for the presence of a tetragonal crystal phase in DDPs obtained from HREM micrographs in CZ-50/50 after 1 h and CZ-68/32 after 15 h.

Particularly for the CZ-50/50 sample after 15 h calcination, HREM micrographs strongly suggest the presence in some crystals of a surface layer of different structure from that of the supporting crystal.

Crystallographic modelling and image simulation work is planned to address this point.

Acknowledgements

The present paper has received the financial support from TMR Program of the European Commission (Contract FMRX-CT-96-0060). R.T. Baker and G.Colón would like to acknowledge their fellowships from TMR Program.

References

[1] B. Harrison, A.F. Diwell, C. Hallett, Plat. Met. Rev. 32 (1988) 73.
[2] J.G. Nunan, H.J. Robota, M.J. Cohn, S.A. Bradley, J. Catal. 133 (1992) 309.
[3] A. Trovarelli, Catal. Rev.-Sci. Eng. 38 (1996) 439.
[4] A. Laachir, V. Perrichon, A. Badri, J. Lamotte, E. Catherine, J.C. Lavalley, J. El Fallah, L. Hilarie, F. Leonormand, E. Quéméré, G.N. Sauvion, O. Touret, J. Chem. Soc., Faraday Trans. 1 87 (1991) 1601.
[5] R.S. Mikhail, R.M. Gabr, R.B. Fahim, J. Appl. Chem. 20 (1970) 222.
[6] J.E. Kubsh, J.S. Rieck, N.D. Spencer, Stud. Surf. Sci. Catal. 71 (1994).
[7] M. Pijolat, M. Prin, M. Soustelle, O. Touret, J. Chim. Phys. 91 (1994) 37.
[8] G.N. Sauvion, J. Caillod, C. Gourlaouen, Rhône-Poulenc, Eur. Patent 0207857 (1986).
[9] T. Ohata, K. Tsuchitani, S. Kitayuchi, Nippon Shokubai Kagaku, Jpn. Patent 8890311 (1988).
[10] N.E. Ashley, J.S. Rieck, Grace WR and Co-Conn., US Patent 484727 (1991).
[11] J. Cuif, G. Blanchard, O. Touret, M. Marczi, E. Quéméré, SAE paper 969106, 1996.
[12] M. Pijolat, M. Prim, M. Soustelle, O. Touret, P. Nortier, J. Chem. Soc., Faraday Trans. 91 (1995) 3941.
[13] G. Colón, M. Pijolat, F. Valdivieso, H. Vidal, J. Kašpar, E. Finocchio, M. Daturi, C. Benit, J.C. Lavalley, R.T. Baker, S. Bernal, J. Chem. Soc., Faraday Trans 94 (1998) 3717.
[14] A. Guinier, in: Théorie et Technique de la Radiocrystallographie, 3^{éme} ed., Paris, 1964, p. 461.
[15] A. Méthivier, M. Pijolat, J. Catal. 139 (1993) 329.